Time-resolved photoelectron spectroscopy of the allyl radical: The lifetimes of the ultraviolet bands

Thomas Schultz and Ingo Fischer

Citation: The Journal of Chemical Physics **109**, 5812 (1998); doi: 10.1063/1.477203
View online: http://dx.doi.org/10.1063/1.477203
View Table of Contents: http://scitation.aip.org/content/aip/journal/jcp/109/14?ver=pdfcov
Published by the AIP Publishing

Time-resolved photoelectron spectroscopy of the allyl radical: The lifetimes of the ultraviolet bands

Thomas Schultz and Ingo Fischer[a)]
Laboratorium für Organische Chemie der ETH Zürich, Universitätstrasse 16, CH-8092 Zürich, Switzerland

(Received 1 June 1998; accepted 10 July 1998)

We report $[1+1']$ picosecond time-resolved pump–probe photoelectron spectra of the UV bands of the allyl radical. The experiments are performed in a molecular beam of allyl radicals, generated by supersonic jet flash pyrolysis. Photoelectron spectroscopy in a magnetic bottle is shown to be a suitable method for investigating the photophysics of organic radicals. Lifetimes were obtained for all vibronic bands between 250 and 238 nm previously assigned by MPI spectroscopy to the electronically excited $B\ ^2A_1$, $C\ ^2B_1$, and $D\ ^2B_2$ states, with values ranging from 20 ps to 9 ps. The nonradiative decay is due to internal conversion to the electronic ground state. Information on the structure of the allyl cation is deduced from the photoelectron spectrum. © *1998 American Institute of Physics.* [S0021-9606(98)02438-6]

I. INTRODUCTION

In this paper we report the lifetimes for a number of vibrational levels in the $B\ ^2A_1$, $C\ ^2B_1$, and $D\ ^2B_2$ electronically excited states of the allyl radical, C_3H_5, as revealed by picosecond time-resolved pump-probe photoelectron spectroscopy.

There are numerous reasons for the interest that the allyl radical, C_3H_5, attracts among chemists. First, it is the smallest unsaturated hydrocarbon radical (π-radical), thus serving as a model system for a whole class of molecules. Second, it is a relatively stable radical that can accumulate in reactive environments, but becomes reactive upon photochemical excitation at relatively low energies as compared to stable molecules. An example of a reactive environment of high technical relevance is a combustion engine, where allyl is assumed to be an important intermediate in propane (C_3H_8) and butane (C_4H_{10})-rich flames.[1] All C_3-hydrocarbon units are believed to be precursors in the formation of soot and polynuclear aromatic hydrocarbons,[2] because two C_3 units can combine to form an aromatic unit, like phenyl-radicals. One can also assume that allyl radicals, formed from partially unburned fuel, are important intermediates in tropospheric chemistry.

Considerable spectroscopic information is available on the energies and symmetries of the electronic states of the allyl system, as summarized in Fig. 1. The ground-state geometry is known with high accuracy from IR diode laser spectroscopy,[3] while the vibrational frequencies were determined by resonance Raman spectroscopy[4] and IR spectroscopy in cryogenic matrices.[5] The location of the electronic A state was derived from an unassigned, but well resolved absorption spectrum.[6] The UV band system starting at 250 nm was studied in detail by absorption spectroscopy,[7] multiphoton ionization,[8–12] and resonance Raman spectroscopy.[4,13,14] Excited state geometries were derived from partially rotationally resolved MPI spectra.[11,12] Although a high oscillator strength of 0.23–0.26 was calculated in a theoretical study for one of the electronic transitions,[15] and also measured in absorption,[16] the complete absence of fluorescence was reported,[4] indicating short lifetimes. The presumably laser-limited linewidth of 1 cm^{-1} in the MPI studies, however, poses a lower limit of 5 ps on the lifetime of the lower vibronic states. Due to their closeness in energy the electronic states are assumed to be strongly mixed, which means that the assignments given in Fig. 1 should be regarded as zero-order. This is confirmed by the appearance of formally symmetry forbidden transitions into several vibrational levels of the B state in the $[1+1]$ MPI spectrum.[11,12] As shown in Fig. 1, the energy of the lowest quartet state was calculated to be at 6.33 eV,[15] approximately 1.2 eV above the D-state origin. Thus it is assumed to be irrelevant for the present study.

In contrast to the spectroscopy, the chemical dynamics and reactivity of the allyl radical upon UV excitation is not understood. Until recently, most of the available experimental information originated from matrix isolation experiments,[17,18] where the reaction products appearing upon irradiation of allyl radicals were identified by their ground state IR spectra. Irradiation at 254 nm,[18] yielded a mixture of allene, propyne, acetylene, methane, and traces of propene, while irradiation at 400 nm supposedly yielded cyclopropyl radicals.[17] Theoretical studies[19] suggested a disrotatory photocyclization upon excitation in the UV bands, a reaction pathway that was supported by the results of a resonance Raman experiment[4,13,14] performed at 224.63 nm, but no direct information on the decay properties of the UV band system is yet available. Thus the results have to be regarded as inconclusive.

In two recent communications we described the application of sophisticated laser techniques to the investigation of the photochemistry of the allyl radical. On the one hand, we applied picosecond time-resolved photoelectron spectroscopy to follow the initial decay of low-lying vibrational levels of the B-state in real time,[20] obtaining lifetimes around 20

a)Author to whom correspondence should be addressed.

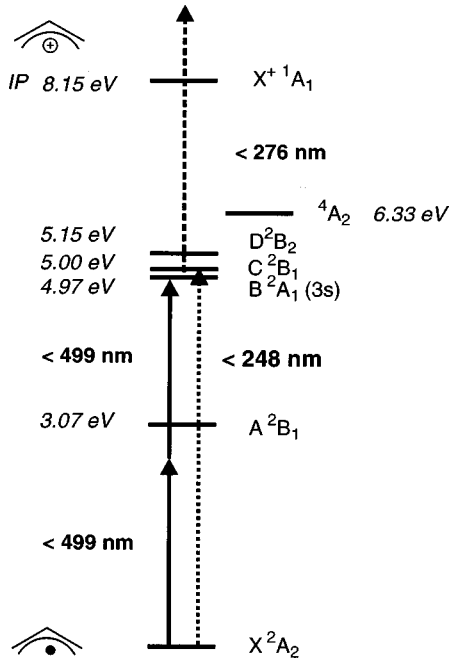

FIG. 1. Location of the electronic states of the allyl radical. In the pump step the UV bands of allyl between 4.99 and 5.21 eV were excited by either one- (dotted arrow) or two-photon (full arrows) excitation and probed by one-photon ionization (dashed arrow).

ps due to internal conversion of the *B*-state. In a different experiment we detected the loss of hydrogen atoms from allyl radicals upon UV excitation[21] by time-resolved ionization of H-atoms with Lyman-α radiation with a rate of 4×10^7 s^{-1}, i.e., on a ns time scale. A statistical analysis of the data revealed that allene formation being the dominant reaction channel is in better agreement with the data than cyclopropene formation.

In this paper we will present a full account of the picosecond time-resolved work, investigating the primary photophysical processes directly after the initial excitation into the UV bands. While in our earlier report we focused on the low-lying levels of the *B*-state we will present here additional data on a large number of vibronic levels of the *B*-, *C*-, and *D*-state up to 238 nm, the whole range observed and assigned in the MPI experiments.[11] As excitation into the *B*-state is formally one-photon forbidden, we relied on two-photon excitation in our earlier experiments, as indicated by the full arrows in Fig. 1. Most of the experiments described here employed one-photon excitation into the *C*- and *D*-state, as well as higher *B*-state levels (dotted arrow in Fig. 1).

Within the last decade time-resolved spectroscopy with short laser pulses proved to be a valuable method to monitor chemical reactions of isolated molecules in real time.[22–24] However, in order to avoid intensity effects, it is necessary to work at low fluences, impeding experiments on transient species, which can only be generated in low number densities. The development of efficient detection schemes, like time-resolved photoionization,[22,23,25] made experiments on molecular[22] and metal clusters[26,27] possible. Photoionization is particularly suitable for studies on systems like hydrocarbon radicals, for which in general no fluorescing states are known. Upon photoionization two species, the ion and the electron, are created. As discussed by several groups in experimental[28–32] as well as theoretical contributions,[33,34] detection of the photoelectrons in a time-resolved experiment can yield additional insight into the intermediate state dynamics that is not available when only the total ion signal is collected. The photoelectron spectrum might evolve in time, even when the total ion yield is almost constant, permitting the detection of electronic energy flow in intersystem crossing or internal conversion.[28,35] A recent experiment on the NO dimer,[36] $(NO)_2$, serves as another example. Here a two-step model for the excited-state fragmentation could be derived from the observation of different timescales for the decay of the ion signal and the change in the photoelectron spectrum. Another advantage of photoelectron detection is the possibility of a background-free detection of time-dependent signals, as will be illustrated below.

Several techniques for the detection of photoelectrons have been employed in time-resolved experiments with short-pulse lasers, such as ZEKE-spectroscopy[29,37–39] or electron time-of-flight spectroscopy.[28,32] Being interested in transient species we chose detection in a magnetic bottle time-of-flight spectrometer, which allows for a very high detection efficiency. The advantages of a magnetic bottle in short-pulse experiments were shown in work on the dynamics of low-lying Rydberg states in NH_3 (Ref. 40) and CH_3I.[41] Just recently the technique was extended to transient species in studies on I_2^- and $I_2^-(H_2O)_x$ clusters.[42] Here we demonstrate the application of time-resolved spectroscopy in a magnetic bottle to medium-sized organic hydrocarbon radicals.

II. EXPERIMENT

A schematic drawing of the experimental setup is given in Fig. 2. The laser system employed in the experiments consists of a titanium–sapphire (Ti:Sa) laser (Spectra Physics Tsunami) with a pulse duration of 1.6 ps (assuming a $sech^2$ pulse shape), pumped by an argon-ion laser. The ps-pulses are amplified at a repetition rate of 10 Hz in a regenerative Ti:Sa amplifier (REGEN, Positive Light) with an additional double-pass amplifier stage to an energy of 4–8 mJ, depending on the wavelength. The REGEN is pumped by the frequency-doubled output of a Nd:YAG laser (Quanta Ray GCR 190). The duration of the amplified pulses lies between 2 and 2.5 ps, assuming Gaussian pulse shape. The system is tunable from 750 to 840 nm, but the range was extended to the blue and near-UV part of the spectrum by doubling in a 7 mm KDP crystal, maintaining the pulse duration as can be calculated from the known group velocity dispersion of the material. By mixing the frequency-doubled output with the Ti:Sa fundamental in a 3 mm KDP crystal, the sum frequency from 250 to 272 nm is produced. Instead of rotating the plane of polarization for one of the beams, we installed the mixing crystal in a 45° angle. The central wavelength and spectral profile of the pulses were determined in a 270 mm monochromator (Acton Research) with a 1800 grooves/mm grating, yielding a wavelength accuracy of ± 0.1 nm.

As evident from Fig. 1 the electronic states of interest in the allyl radical lie outside the tuning range of the laser sys-

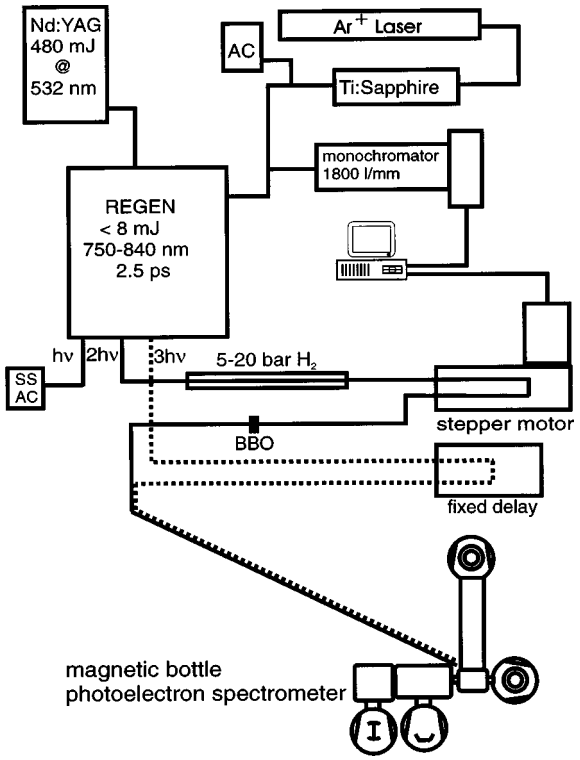

FIG. 2. Schematic drawing of the experimental setup, based on a Ti:sapphire laser system, amplified at 10 Hz, with a pulse duration of 2–2.5 ps and mJ-energies. In order to extend the tuning range of the system to pump the UV bands of allyl, the second harmonic output was Stokes-shifted in H_2, while the frequency-tripled output served as the probe pulse. For the $[1+1']$ experiments the Stokes shifted radiation was frequency doubled in a BBO crystal. The two pulses were recombined and focused into the ionization region of a molecular beam apparatus equipped with a magnetic bottle photoelectron spectrometer.

tem. In order to pump the UV bands in allyl to the blue of 250 nm, we utilized the technique of stimulated Raman scattering (SRS) and shifted the frequency-doubled Ti:Sa pulse in a high-pressure hydrogen cell. A detailed description of the process, including a characterization of the Raman-shifted pulse, was given in an earlier publication.[43] Here we just note that the duration of the pulse shortens by a factor of 2, maintaining the time-bandwidth product of the input pulse ($\Delta\tau\times\Delta\upsilon\approx 0.7$), thus leading to a spectrally broadened pulse with a halfwidth of $\approx$15–18 cm^{-1}. The energy of the pump pulse was controlled by adjusting the hydrogen pressure in the cell between 5 and 20 bar. For two-photon excitation of the *B*-state (full arrows in Fig. 1) the first order Stokes-shifted light, S1, around 499 nm, corresponding to a Ti:Sa fundamental of 826.6 nm, was used directly. For one-photon excitation of the *B*-, *C*-, and *D*-state (dotted arrow in Fig. 1) the S1 was frequency doubled in a 1 mm BBC crystal, in order to produce radiation between 250 nm and 238 nm, increasing the bandwidth to approximately 20–25 cm^{-1}.

The frequency tripled radiation from the Ti:Sa system served as the probe pulse, as indicated by the dashed arrow in Fig. 1. As in the present setup both pulses were derived from the same fundamental, the wavelength of the probe pulse depended on the chosen pump wavelength and varied for the experiments on different vibronic states. We attenuated the energy of the probe pulse in order to minimize one-color background signal. Typically, energies of 1 μJ or less were used for both, pump and probe, in the $[1+1']$ experiments, whereas in the $[2+1']$ experiments pump energies around 20 μJ and probe energies from 2 to 10 μJ were employed.

In all experiments the relative timing of the two pulses was controlled by sending the pump beam to a retroreflector mounted on a computer-controlled stepper motor (Aerotech ATS 02040). Typically one data point was taken every picosecond. The two beams were recombined with a dichroic mirror and focused collinearly by a 500 mm quartz lens into the ionization region of a magnetic bottle time-of-flight photoelectron spectrometer, leading to intensities on the order of 10^{11} W/cm^2 in the $[1+1']$ experiments. In the $[2+1']$ experiments the lens was positioned in such a way that the probe beam focused slightly before and the pump beam slightly after the ionization volume. We estimate the intensities to be similar to those in the $[1+1']$ experiments.

The details of the spectrometer (Applied Laser Technology) were already described before.[44,45] The advantage of a magnetic bottle as compared to other electron detection techniques is the high detection efficiency of 30%–50%, making it a suitable device for experiments on transient species that can only be produced with low number density. The tradeoff is a modest energy resolution of typically 15 meV for low energy electrons, although experiments with significantly better resolution were reported.[46] In our work we detected comparably fast electrons, resulting in an inferior resolution of typically 30 meV. The signals were read out, averaged over 200 shots, digitized in a storage oscilloscope (LeCroy 9450) and transferred from there into a personal computer. The start signal for the detection was established by a photodiode mounted behind the exit window of the spectrometer. The signals were not corrected for laser power.

A clean beam of allyl radicals was obtained by supersonic jet flash pyrolysis[47] of 1,5 hexadiene seeded in 1 bar of helium. It was obtained from Fluka and used without further purification. The details of the radical source, mounted on a General Valve solenoid with a 0.8 mm nozzle, are described in the literature.[48] Number densities of more than 10^{14} radicals per cm^3 can be obtained at the source exit, which yields around 10^{10} radicals per cm^3 in the ionization region. The source region is pumped by a 235 ft^3/min roots blower, while the main chamber, separated by a skimmer, is equipped with a 2400 ℓ/s diffusion pump. An additional 200 ℓ/s turbopump is attached to both, the ionization region, and the detector region in the magnetic bottle, in order to achieve differential pumping. Typical operating pressures were on the order of several 10^{-5} Torr in the ionization region and around 1×10^{-6} Torr in the magnetic bottle

Mass spectra were obtained in the same spectrometer by applying up to 800 V to an electrode mounted on the lower poleface of the magnetic bottle. However, the detection efficiency is significantly reduced as compared to electron detection.

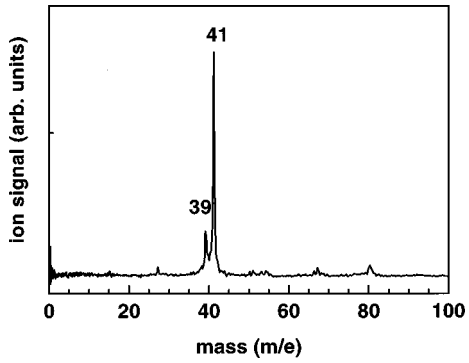

FIG. 3. The mass spectrum recorded via the $B\ 0_0^0$ state at 499 nm is dominated by a peak at $m/e=41$, corresponding to allyl. A smaller peak appears at $m/e=39$ due to fragmentation in the ion. Note the very small signal from the precursor, 1,5 hexadiene, at $m/e=82$. All signals went away when the pyrolysis source was turned off.

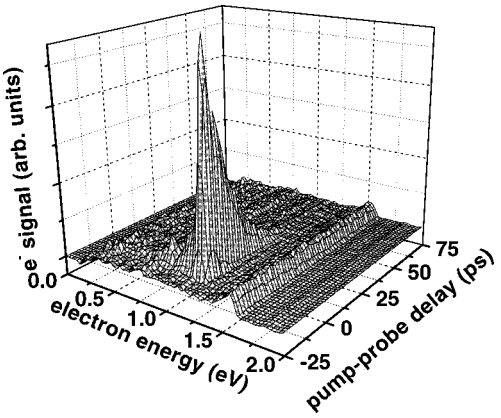

FIG. 4. The complete time-resolved photoelectron spectrum from the $C\ 0_0^0$ state at 248.1 nm. The time-dependent signal due to $[1+1']$ ionization, as well as a time-independent signal due to a $[1+1]$ process can be recognized.

III. RESULTS AND DISCUSSION

A. Mass spectra

In experiments on transient species it is important to establish the identity of all species that might contribute to the time-dependent signals. Therefore mass-spectra were recorded in our spectrometer. A spectrum recorded on the $B\ 0_0^0$ state of allyl, excited by a two-photon pump process at 499.3 nm, is given in Fig. 3. As visible, it is dominated by a peak at $m/e=41$, which corresponds to the mass of allyl, with another smaller signal at $m/e=39$. Since the observed lifetime of this peak as determined from time-resolved mass spectroscopy is identical to the one observed for allyl, we assign this peak to fragmentation in the allyl cation due to absorption of a second probe photon, leading to the formation of $C_3H_3^+$. The reaction of allyl cation to cyclopropenyl cation, the global minimum on the $C_3H_3^+$ potential energy surface, and H_2 is associated with a heat of reaction, ΔH_R, of only 30 kcal/mol. We note, that the cyclopropenyl cation plays an important role in the chemistry of the interstellar space as a precursor of $C_3H_2^+$, the most abundant hydrocarbon cation in space. Only a very small signal appears at $m/e=82$, the mass of the precursor, 1,5 hexadiene, proving that it is not ionized under our experimental conditions, and thus does not contribute to the signal in the photoelectron spectra discussed below. In addition it was ensured in each experiments that the signal vanished upon turning off the heat at the pyrolysis source, demonstrating that no photolytic cleavage of the precursor occurred. We regard it as an important advantage of pyrolysis that precursors can be selected that are not susceptible to photolytic cleavage at the wavelength employed in the pump–probe experiment. In conclusion, the mass spectrum indicates that we generate a clean beam of allyl radicals under our conditions. Mass spectra recorded via other intermediate states are very similar in appearance.

B. [1+1′] photoelectron spectra, time dependence, and decay traces

Time-resolved experiments are typically performed as pump–probe experiments, with a pump-laser exciting an intermediate state that evolves in time. The excited-state population is then monitored in real time by a time-delayed probe pulse that projects the intermediate state dynamics onto a final state. In the experiments described here, this final state is the ground state of the allyl cation. We obtain a time-dependent signal from the evolving intermediate state that is due to detection of the electrons formed in the ionization process as a function of the pump–probe delay.

For each vibronic band photoelectron spectra were recorded every ps over a pump–probe delay range of around 100 ps. A complete scan gives rise to a three-dimensional spectrum, like the one from the *C*-state origin, depicted in Fig. 4. Here pulses with a wavelength of 248.1 nm and 274.3 nm for pump and probe, respectively, were employed, corresponding to a total energy of 9.52 eV. In such a scan the excited state population can be monitored by following the intensity of a given band in the photoelectron spectrum over the delay time. The advantages of photoelectron spectroscopy as a final-state selective detection technique are best illustrated in the photoelectron spectra recorded at pump–probe delays $\Delta t=0$ and $\Delta t=-10$ ps (i.e., with the probe laser arriving in time either together with, or before the pump laser) given in the upper and lower trace of Fig. 5. Both

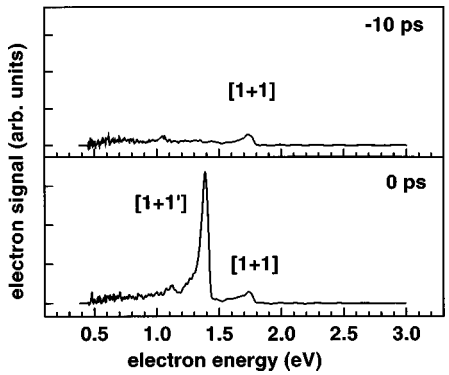

FIG. 5. The two photoelectron spectra recorded at $t=-10$ ps (upper trace) and $t=0$ (lower trace) were obtained from the full scan in Fig. 4. As visible, the time-dependent $[1+1']$ signal is well separated from the time-independent $[1+1]$ signal, permitting a background-free detection of the former. Note that the order of the process can be deduced from the electron energies.

spectra were obtained from the full scan, given in Fig. 4. A sharp time-dependent peak, with some vibrational structure being apparent, is visible at 1.37 eV electron excess energy when the two lasers are overlapped in time, due to a $[1+1']$ ionization process. In addition, the pump laser alone can ionize the molecule in a $[1+1]$ process, producing an unwanted time-independent background signal, that is present in both spectra around 1.8 eV. As the excess energy transferred to the electron is different for the two processes, the signals associated with them appear at a different place in the photoelectron spectrum, allowing to separate the time-dependent from the time-independent contributions, as long as the energies of the two photons are sufficiently different from each other. In this sense photoelectron spectroscopy is a background-free detection technique. It is noteworthy that background signals are observed from the pump laser alone, despite a pulse energy of only 1 μJ, illustrating the problem of interfering multiphoton processes in short-pulse spectroscopy. Although in the present example the time-independent signals are relatively small compared to the time-dependent ones, for several other bands they became equal in magnitude at later delay times. This lead to a significant noise level in the time-resolved mass spectra and subsequently to larger uncertainties in the lifetimes determined by collecting the total ion signal. Another advantage of photoelectron spectroscopy is the easy determination of the order of the time-dependent process directly from the electron energies, ensuring that the signal originates indeed from a $[1+1']$ process. A hypothetical $[2+1']$ process would be associated with very fast electrons, arriving at the detector significantly earlier than the electrons formed in the $[1+1']$ or $[1+1]$ processes. If only the total ion signal is collected, it is more difficult to say from which process the signal originates. This issue will be further discussed below in the Appendix, where we describe the determination of an instrument response function from a signal due to a higher order process, which appeared in the time-resolved photoelectron spectrum of the S_1 state of pyridine.

To monitor the population decay in the intermediate state, i.e., to obtain lifetimes, the intensity of the major time-dependent peak in the photoelectron spectrum was integrated and the integral plotted as a function of the pump–probe delay. An example of the resulting decay curve is given in the upper trace of Fig. 6, with the solid line being a fit to the data points that represents a convolution of the instrument response function of 4 ps with a monoexponential decay. The time constant obtained this way for the population flow out of the *C*-state origin was 15 ps.

In principle the lifetimes and nonradiative decay properties depend not only on the vibrational, but also on the rotational state. Such a rotational dependence was for example reported in a ps time-resolved study of predissociation lifetimes in the *B*- and *C*-state of ammonia, where significantly different lifetimes were reported for high or low $J'K'$ values.[40] In the case of allyl with two small rotational constants[3] ($B''=0.346\ \mathrm{cm}^{-1}$, $C''=0.290\ \mathrm{cm}^{-1}$) it is not possible to excite individual *J*-states even with pulsed ns-dye lasers. On the other hand, due to the relatively large constant $A''=1.802\ \mathrm{cm}^{-1}$, the *K*-structure was partially resolved in the ns-MPI spectra, permitting a simulation of the rotational band contours. As allyl is a near-prolate asymmetric rotor ($\kappa\approx-0.9$), K_a can be used as an approximate rotational quantum number. With our broad excitation bandwidth of more than 20 cm^{-1} we will always excite a superposition of several K_a'-states. Nevertheless it is possible to distinguish between excitation to a low-K_a' or high-K_a' superposition. While the decay curve given in the upper trace of Fig. 6 corresponds to excitation to the $C\ 0_0^0$ bandhead, the curve given in the lower trace corresponds to excitation to high K_a' states, originating from $K_a''\approx12$. Apart from a smaller overall signal, and a subsequently inferior signal to noise ratio, the decay curves look very similar and yield the same time constant of 15 ps. Therefore we conclude, within the restrictions discussed above, that there is no significant influence of the rotational state on the decay of the *C*-state origin.

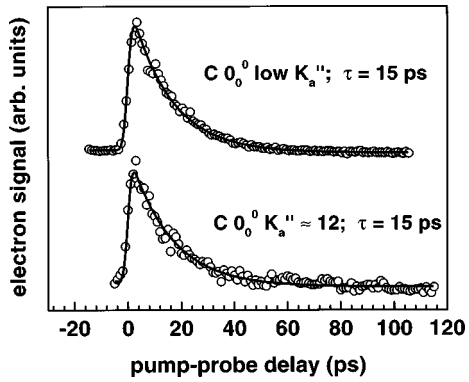

FIG. 6. The decay of the *C*-state origin. The signal was obtained by integrating the major peak given in Fig. 4, and plotting it as a function of the pump–probe delay. The fit constitutes a convolution of a monoexponential with a time constant of 15 ps and a Gaussian of 4 ps FWHM, representing the instrument response function. No difference was found between excitation of the $C\ 0_0^0$ bandhead (upper trace) and high K_a'-levels originating from $K_a''\approx12$ (lower trace), indicating the absence of rotational effects on the decay.

In the same manner we obtained lifetimes for all vibronic bands between 250 and 238 nm that were assigned in the MPI spectra, with some more examples given in Fig. 7. The values for the lifetimes of all bands, obtained at the band maximum, are summarized in Table I together with the excitation wavelengths and assignments reported in Ref. 11. While the value for the *B*-state origin was taken from the $[2+1']$ experiments reported earlier, all other lifetimes were determined in $[1+1']$ experiments. We note that most values constitute an average over several scans. The overall accuracy of the lifetimes is estimated to be around ±1 ps, although for some states, in particular the $C\ 0_0^0$, it is certainly much better. An overall decrease of the lifetime with increasing excitation energy is visible, but no sudden jump is apparent, suggesting that the dominating nonradiative decay channel operates on all *B*- and *C*-state vibronic levels in the same manner. At the blue end of the energy range studied, the lifetime becomes as short as 9 ps for the $D\ 7_0^1$ band. In this range, the signal intensity for the vibronic transitions reported in the nanosecond MPI spectrum becomes rather small, in contrast to the findings of absorption experiments, where the absorption cross section continues to grow down

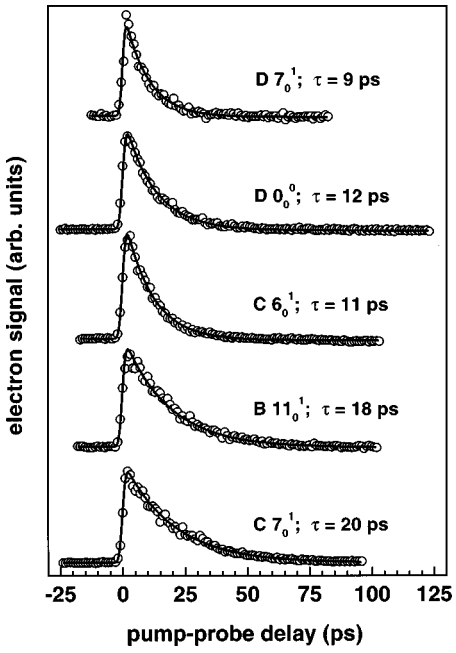

FIG. 7. Decay traces for a selected number of vibronic states of the the allyl UV band system. The lifetime decreases to the blue, reaching a value of 9 ps for the $D\ 7_0^1$ state, the bluest band assigned in the earlier MPI studies.

to 224 nm. From our results we conclude that due to the decreasing lifetimes, ionization can no longer compete efficiently with the nonradiative decay of the states in experiments with ns-laser pulses, leading to successively smaller signals in the earlier MPI experiments.

In our earlier communication on the dynamics of low-lying levels of the $B\ ^2A_1$ state, we suggested that the nonradiative decay is due to internal conversion either directly to the ground state, or via the *A*-state. We are convinced that similar arguments also apply to the vibronic states discussed here and the decay is also due to internal conversion. Alternative channels can be ruled out for the following reasons: (a) intersystem crossing is not possible, because the lowest quartet state is energetically not accessible in the range of excitation energies discussed in this paper, see Fig. 1; (b) dissociation into C_3H_4 plus a hydrogen atom does occur, but on a nanosecond time scale, as shown recently.[21] Thus the decays reported here cannot be due to direct or predissociative hydrogen loss from the UV states. (c) A third possibility would be excited state isomerization, leading to the formation of either cyclopropyl or methylvinyl radical. Photocyclization in agreement with the Woodward–Hoffmann rules was suggested by theoretical studies[19] and resonance Raman experiments.[4] At the excitation energies present in our experiment, the cyclopropyl radical would lose a hydrogen atom and form the closed-shell molecule cyclopropene. In our recent nanosecond experiments,[21] investigating the H-atom product of the unimolecular dissociation of allyl radicals, no indication for cyclopropene formation was found. Thus we conclude that under our conditions photocyclization does not constitute an important decay channel for the UV bands of allyl. However, we want to emphasize that the experimental evidence for this channel was obtained from resonance Raman experiments performed at 224.63 nm, significantly further to the blue. We cannot rule out that photocyclization might become important in this wavelength range. A second isomeric intermediate that might be formed is the methylvinyl radical. Indeed, evidence for the appearance of this species in the photodissociation of hot ground state allyl radicals will be presented in a forthcoming paper.[49] However, there are several strong arguments against an excited state isomerization in the UV bands. First, the statistical analysis of the nanosecond data[21] is in agreement with a reaction from a hot ground state. Second, two different pathways for the $C_3H_5 \rightarrow C_3H_4+H$ reaction with different rates on the ns-time scale were identified in the nanosecond experiments, the faster one being site-specific allene formation, associated with the loss of the central hydrogen atom. No mechanism proceeding via an excited state isomer can be envisioned to be in agreement with this site-specificity. There would be the possibility to have two different decay processes from the excited states, but all decay traces investigated can be well fitted by a monoexponential function, forcing us to the conclusion that there is only one primary decay channel of the UV bands. This means that the branching into two reaction channels observed in the nanosecond experiments,[49] occurs on the ground state surface. The only decay channel from the UV bands that provides access to several different reaction channels is internal conversion to the ground state, producing hot ground state radicals with enough internal energy to overcome the activation barriers for several reaction channels.

TABLE I. The peak positions (band maxima) and assignments for the different UV bands, taken from Ref. 11, are given with the lifetime obtained from the time-domain experiments. The lifetime for $B\ 0_0^0$ was determined in a $[2+1']$ experiment, while all other values were obtained from $[1+1']$ experiments.

Wavelength (nm)	Assignment	Lifetime (ps)
249.7	$B\ 0_0^0$	20
248.1	$C\ 0_0^0$	15
247.4	$B\ 7_0^1$	20
246.3	$B\ 12_0^1$	19
246.1	$B\ 9_0^1$	20
245.8	$C\ 7_0^1$	20
245.0	$B\ 7_0^2$	15
243.7	$B\ 11_0^1$	18
243.5	$C\ 7_0^2$	18
243.1	$B\ 10_0^1$	16
242.1	$C\ 6_0^1$	11
241.9	$B\ 17_0^1$	11
241.4	$C\ 5_0^1$	13
240.6	$D\ 0_0^0$	12
239.1	[a]	10
238.4	$D\ 7_0^1$	9

[a]This band was reported, but not assigned in Ref. 11.

For the internal conversion of the UV bands two different pathways are possible, either decay directly to the ground state, or a two-step process via the *A* state. The rate of nonradiative decay, $k_{i\rightarrow f}^{\mathrm{IC}}$ as given by Fermi's Golden Rule[50]

$$k_{i\rightarrow f}^{\mathrm{IC}} = \frac{2\pi}{\hbar}\,\beta^{\mathrm{IC}}\langle\chi_i|\chi_f\rangle^2\rho(E) \qquad (1)$$

is governed by two factors, the density of states, $\rho(E)$, and the Franck–Condon factors between the coupled vibronic levels, $\langle \chi_i | \chi_f \rangle$, assuming constant coupling matrix element β^{IC}. The vibrational density of states in the ground state at this energy is on the order of $10^{10}/cm^{-1}$ while the one for the *A*-state is more than four orders of magnitude smaller, thus favoring a direct conversion to the ground state. On the other hand, conversion via the *A*-state should be favored by the smaller energy gap and the better vibrational overlap. As the *X*- and *A*-state are very similar in geometry, IC to the ground state would result in a higher degree of vibrational excitation than IC to the *A*-state, leading to less favorable Franck–Condon factors in expression (1). We note that the rate for the nonradiative decay lies between 5×10^{10} s^{-1} and 1×10^{11} s^{-1} and is thus remarkably slow for a higher excited states of a molecule that size, probably due the large energy gap between the UV bands and the lower-lying states of around 2 eV or more between the *C* and the *A* state and 5 eV or more between the *C* and the *X* state.

In principle one would expect a signal from a lower electronic state to grow in the time-resolved photoelectron spectrum with increasing delay time.[28,35] However, no such signal could be identified in our time-resolved photoelectron spectra. This can be explained by the large degree of vibrational excitation present in the lower electronic states after the internal conversion, in particular in the electronic ground state, due to the large energy gap. The vibrationally highly excited states will have poor Franck–Condon factors with the low-lying ionic states accessible in this experiment, because the excess energy available in the ion ranges from 1.3 eV for the *B*-state origin to 1.7 eV for the $D\ 7_0^1$ state, the highest state investigated. As the wavelength of the probe pulse depended on the chosen pump-wavelength (see above) we were not able to probe a larger range of the potential energy surfaces. Future experiments employing two independently tunable lasers will address this issue. For ionization from the *A*-state the situation is more favorable, but it is likely that a highly excited *A*-state, populated by IC from the UV states, has itself a fast nonradiative decay that cannot be time-resolved in our experiment.

Another reason for the absence of a signal from a lower electronic state could be an unfavorable electronic matrix element.[36] In a one-electron picture the *A*-state would correspond to a $[(b_1)^1(a_2)^2]$ configuration, while the *C*-state would correspond to a $[(b_1)^2(a_1)^1]$ configuration. Thus one might expect a poor electronic matrix element between the *A*-state and the $[(b_1)^2]$ cationic ground state. However, earlier theoretical work indicates that the *A*- and the *C*-state, being both of B_1 symmetry, are mixed, with each configuration contributing to both states.[15] Thus unfavorable electronic matrix elements are not expected to be important for the ionization of excited states of allyl.

In order to get more insight into the mechanism of the decay of the UV bands, the lifetimes of the UV bands are plotted in Fig. 8 as a function of excitation energy, with the inverse vibrational density of states of the electronic ground state, $(\rho_{vib})^{-1}$, given for comparison. Overall the decrease in the lifetimes is approximately proportional to the density of states, indicating a decay governed by $\rho(E)$, and thus by

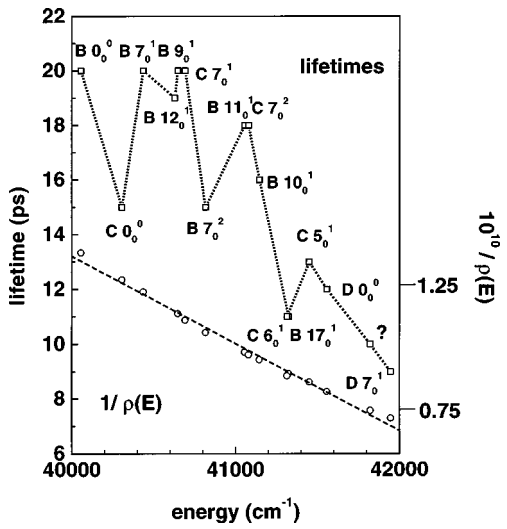

FIG. 8. Comparison of the measured lifetimes of the different vibronic states (squares) with the inverse vibrational density of states of the electronic ground state, $\rho(E)$ (circles). The decrease in the lifetimes is approximately proportional to the increasing density of states. However, the $C\ 0_0^0$ and maybe the $B\ 7_0^2$ bands deviate from this relation, showing that factors other than the density of states become important.

conversion directly to the ground state. Two interesting features can be observed: Vibronic bands that are very close to each other have very similar lifetimes, as evident for the tiers of states around 40.630 cm^{-1} ($t=19-20$ ps), 41.060 nm^{-1} (18 ps), or 41.320 cm^{-1} (11 ps). This confirms the assumption of a very strong coupling of the states, which was suggested in the earlier MPI work, based on the appearance of the formally one-photon forbidden *B*-state bands in the [1+1] spectra. The other remarkable feature is the pronounced deviation of the $C\ 0_0^0$ state from this linear relation with the density of states. The deviation might also be present for the $B\ 7_0^2$ band, but given the error bars of ±1 ps on the lifetimes it is not entirely clear. Interestingly both are relatively isolated bands, separated by more than 100 cm^{-1} from their next neighbor, indicating that the coupling between neighboring states leads to a lengthening of the lifetime. So factors other than the density of states do play a role for the radiationless decay of at least some of the states. It might be possible, for example, that *B*-state contributions lead to a lengthening of the lifetime of formally *C*-state levels, or that additional interactions with the *A*-state modulate the electronic matrix elements β^{IC} for the decay into the ground state. We note, however, that our nanosecond experiments[21,49] indicate no change in the photodissociation dynamics when different UV bands are initially excited.

Information on the relative importance of the density of states and the FC-factors is available from experiments on isotopic species. Deuteration of allyl should on the one hand increase the density of states, but on the other hand lead to less favorable FC-factors.[51] Such experiments that might give additional insight into the decay mechanism will be carried out in the near future.

C. Structure of the [1+1′] photoelectron spectra

For a discussion of the intermediate state dynamics it is important to have sufficient information on the final state on

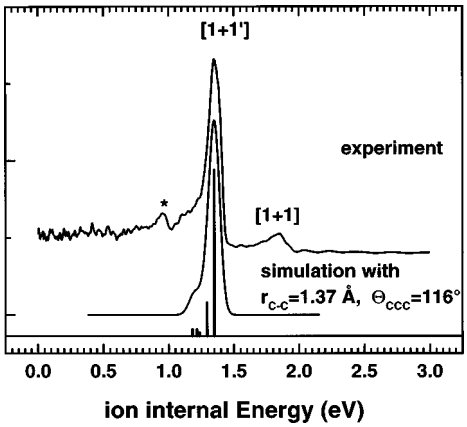

FIG. 9. The photoelectron spectrum from the *C*-state origin (top trace), compared with a simulated spectrum (center trace), obtained by convoluting the stick spectrum in the bottom trace with a Gaussian with a FWHM of 30 meV. In order to simulate the low energy shoulder of the major peak, the C–C bond length had to be refined. The best fit was obtained for r(C–C)=1.37 Å and Θ_{CCC}=116°. Frequencies of 1350, 1080, and 450 cm^{-1} were employed for the ionic modes v_5^+, v_6^+, and v_7^+. For the other parameters see text.

which the dynamics is projected on. As the ionic ground state is known for many molecules from steady-state photoelectron spectroscopy it often constitutes a suitable choice as a template for studying intermediate state dynamics. In earlier photoelectron work on the allyl radical by Houle and Beauchamp,[52] an adiabatic ionization potential of 8.13±0.02 eV was reported. A single strong progression of 420 cm^{-1} was observed, but not assigned. The closeness of the adiabatic and the vertical ionization potential indicates that the geometry change upon ionization is small, as expected for the ejection of a formally nonbonding electron.

Compared to the photoelectron spectra recorded from the neutral ground state, our spectra are considerably simplified by the selection of an intermediate state, removing any contribution from hot bands. As the overall shape of the spectra does not change with the pump–probe delay it is possible to analyze them in order to obtain additional information on the ionic ground state. The advantages of photoelectron spectroscopy from selected intermediate states as compared to the ground state were discussed in detail by Kimura[53] several years ago. We will now examine the spectrum obtained from the $C\ 0_0^0$ state, given in Fig. 9, which is dominated by a single peak, with some broadening on the low energy side, due to vibrational excitation in the ion. One other well-separated band, shifted by ≈0.3 eV in energy, is visible. As the total energy is 9.52 eV, we calculate an ionization potential of 8.15 eV, in good agreement with the value of 8.13 eV from Houle and Beauchamp,[52] given that our error bars are also estimated to be around 20 meV. The absence of a strong progression suggests an ionic geometry which is very similar to the *C*-state. The major change in geometry upon excitation from the ground state to the *C*-state origin is a decrease in the CCC angle Θ_{CCC} from 121° to 116.5°, accompanied by a slight decrease of the C–C bond length from 1.3869 Å to 1.385 Å. Minsek and Chen[12] reported an excellent fit to the MPI spectra with those two values, keeping the other angles and bond lengths at their ground state values. As the 420 cm^{-1} progression reported by Houle and Beauchamp[52] is absent in our spectrum, it is reasonable to assume a Θ_{CCC} similar to the *C* state and assign it to the CCC bending mode v_7^+. This is confirmed by the photoelectron spectrum from the $C\ 7_0^1$ state, yielding an IP that is approximately 450 cm^{-1} higher in energy. We note, that a frequency determination by comparing the energy of the dominating peak in different spectra is relatively inaccurate, because the errors of 20 meV in the energy calibration for each spectrum can add up. In addition, different CCC bond angles were reported for the higher *B*- and *C*-state levels, so additional activity in the ionic bending mode v_7^+ can be expected, further complicating an unambiguous identification of the origin.

We analyzed the excited state photoelectron spectrum from the *C*-state origin performing a Franck–Condon simulation, following the approach outlined by Chen.[54] This state is the one examined in most detail in the ns-MPI experiments, so a good geometry was available from this work. A starting geometry for the ion was obtained from *ab initio* calculations, using the GAUSSIAN suite of programs[55] (MP2 calculation with a 6-31G** basis set), which was then refined to achieve a good fit to the spectrum. Several other parameters necessary for the Franck–Condon simulations, like force constants and atomic displacement matrices, were obtained from *ab initio* calculations of the neutral ground state. This simplification seems justified because these parameters depend predominantly on the atomic masses and change little upon electronic excitation. We chose the spectrum recorded at the maximum signal intensity, because the shape does not change with increasing pump–probe delay, see above.

In Fig. 9 the photoelectron spectrum from the $C\ 0_0^0$ is given in the top trace, with the best fit given for comparison in the center trace. We found that slight changes in the CCC bond angle Θ_{CCC} had little effect on the shape of the spectrum and could not reproduce the shoulder on the low energy side. Changes in the C–C bond length, on the other hand, had a pronounced effect on the spectrum. The stick spectrum, given in the bottom trace of the figure, was obtained with $r_{(C-C)}$=1.37 Å and Θ_{CCC}=116°, with the other parameters fixed at the *ab initio* values of 1.0802 Å (central C–H bond), 1.0824 Å (C–H exo), 1.0836 Å (C–H endo), 121.7° (CCH exo), and 120.78° (C–H endo). It was convoluted with a Gaussian with a FWHM of 30 meV to yield the simulated spectrum in the center trace of Fig. 9. The small geometry change leads to some vibrational activity in the modes v_5^+ (CH_2 rocking), v_6^+ (CCC stretch) and v_7^+ (CCC bend) with vibrational frequencies of 1349, 1080, and 452 cm^{-1}, respectively, as obtained from the calculations. It should be noted that the *ab initio* frequencies are in general too high. In calculations of the allyl ground state we found a scaling factor of 0.94 to yield good agreement between the calculated and the observed frequencies, leading to values of 1270, 1015, and 423 cm^{-1} for the three modes.

With the *ab initio* value of $r_{(C-C)}$=1.3826 Å and Θ_{CCC} =117.6° the shoulder on the low energy side could not be reproduced, with $r_{(C-C)}$ shortened further to 1.365 Å it ap-

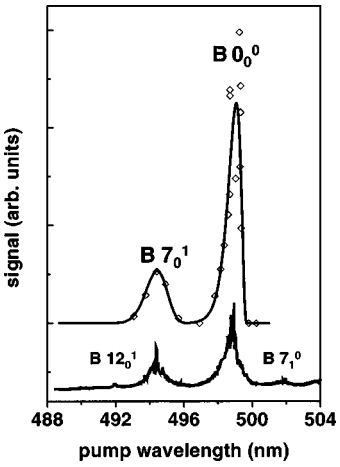

FIG. 10. By tuning the laser system and recording the signal around $t=0$, a $[2+1']$ spectrum of the *B*-state was obtained (upper trace). The experimental data points are given as open diamonds, with the solid line being a smoothed curve, drawn in to guide the eye. The published $[2+2]$ MPI spectrum, given for comparison in the lower trace, is well reproduced.

pears with too high an intensity in the simulation as compared to the experiment.

We already noted the appearance of another relatively broad, time-dependent band in the discussion of the $C\ 0_0^0$ state, marked with an asterisk in Fig. 9. This band is present in all spectra, shifted by 0.3–0.5 eV to lower excess energies from the maximum and a decay time that is always identical to the one of the dominant band. Such a band could in principle be assigned to the fundamental or first overtone of a C–H stretching vibration. However, the available data on the geometry of the excited states and the ionic ground state do not support such an assignment. Therefore we assume that the signal is due to a higher order process. A possible explanation can be deduced from the mass spectrum presented in Fig. 3, which shows the presence of $C_3H_3^+$, formed by fragmentation of allyl cation. Such a dissociative ionization due to a $[1+2']$ process might be accompanied by photoelectrons with a broad distribution of energies and thus be responsible for this band.

D. [2+1′] photoelectron spectra of the $B\ ^2A_1$ state

As mentioned above, one-photon excitation from the $X\ ^2A_2$ ground state into the $B\ ^2A_1$ state is formally forbidden by symmetry. Nevertheless bands formally assigned to the *B*-state can be observed due to the strong mixing of the electronic states in the UV region. However, for low-lying vibrational states, in particular the *B*-state origin, the signals become quite small and are better studied in a $[2+1']$ process. In our earlier communication a lifetimes of 20 ps for the $B\ 0_0^0$, derived from $[2+1']$ experiments, was reported. In those experiments we investigated the whole range studied before by $[2+2]$ MPI spectroscopy by tuning our picosecond laser system. The resulting spectrum is depicted in the upper trace of Fig. 10, with the *y*-axis representing the pump–probe signal at $t=0$. The experimental data points are given as open diamonds, while the solid line represents a smoothed curve, drawn to guide the eye. The $[2+2]$ nanosecond-MPI spectrum[12] is given in the lower trace of the figure for comparison. It is evident that the two spectra match very well and that the picosecond spectrum goes down to zero in between the two bands that dominate the ns-spectrum. This is another confirmation for the identity of the transients reported. The additional features due to the $B\ 12_0^1$ band and the $B\ 7_1^0$ hotband present in the ns-spectrum could not be detected in the ps-experiments, due to the small absorption cross section and the relatively cold molecular beam, respectively. For the $B\ 7_0^1$ band a lifetime of 16 ps with relatively large error bars was reported before. We consider the value of 20 ps obtained in the $[1+1']$ experiment as more accurate.

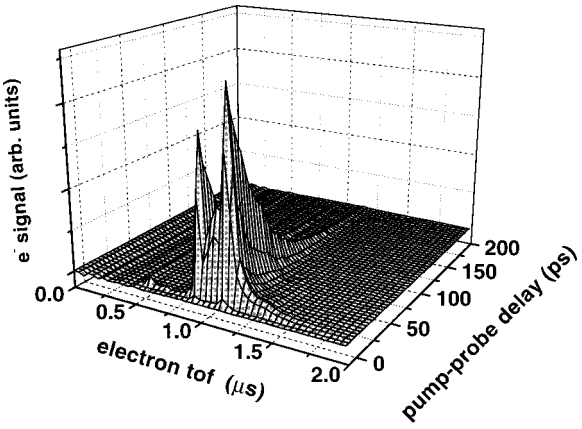

FIG. 11. Time-resolved photoelectron spectrum of the $S_1\ 6a_0^2$ state of pyridin, recorded for calibration of our setup. Note the presence of a small peak around $t=0$, at an electron time-of-flight of 550 ns.

E. [1+2′] photoelectron spectra of pyridine

In order to characterize our experimental setup we carried out time-resolved experiments on the S_1 state of pyridine, which is known to decay by internal conversion to the ground state. The lifetimes of several vibrational levels were determined before in a series of experiments using single photon counting.[56] In our study we pumped the S_1 state with the third harmonic output from the Ti:Sa laser and ionized subsequently with two second harmonic photons. A complete scan for the first overtone of the $6a$ vibration, $6a_0^2$, pumped at 278.8 nm and probed with two photons of 418.2 nm is given in Fig. 11. The time-dependent band shows extensive vibrational structure, with identical time dependence, that we could not yet assign, due to two reasons. First, there is only very little information available on the pyridine cation, and second, our analysis is complicated by the two-photon probe process that in principle permits an influence of highly excited Rydberg-states populated after absorption of the first probe photon. In Fig. 12 a decay trace for the $6a_0^2$ is given, which is fitted with an exponential with a decay constant of 32 ps. This has to be compared with the reported literature value[56] of 38 ps, obtained in the above-mentioned experiments, which was deconvoluted from an instrument response function of 70 ps. We regard the agreement as satisfactory, with our result being probably more accurate.

Upon inspection of the spectrum in Fig. 11, one finds an additional time-dependent signal, appearing around 0.55 μs, at high electron kinetic energies. As visible from its time-

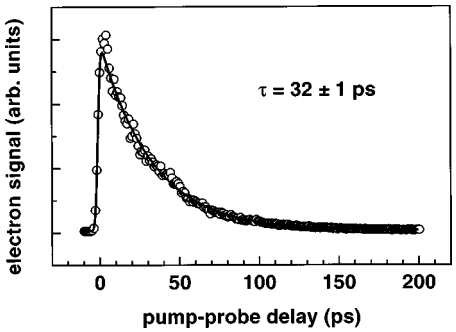

FIG. 12. The decay trace for the $S_1\ 6a_0^2$ state, obtained from the spectrum in Fig. 11, with a lifetime of 32 ps. It is known that the S_1 state of pyridin decays by internal conversion to the ground state.

dependence, given in Fig. 13, it is symmetric with respect to the pump–probe delay. It can be identified from its time-of-flight as being due to a process in which one photon of 278.8 nm and three photons of 418 nm are absorbed, i.e., either a $[1+3']$ or, less likely, a $[3'+1]$ process. If the total ion signal was collected, such a higher-order process would contribute to the signal, possibly complicating the analysis of the data. With a differential, final state selective detection technique, like photoelectron spectroscopy, the contributions from different processes can be separated and assigned to the order of the process. In addition this signal permits the determination of the absolute zero in time, as well as an approximate determination of the cross-correlation function from the full-width at half-maximum. As the signal measured for the decay of the $S_1\ 6a_0^2$ state is due to a process of different order, $[1+2']$ instead of $[1+3']$, the cross correlation (cc) obtained from the $[1+3']$ process, is only an approximation to the instrument response function for the $[1+2']$ process. However, as the width of the both, the cross correlation for the $[1+2']$ and the $[1+3']$ process, is dominated by the width of the Ti:Sa third harmonic, we assume that the two values are very similar. This way we determined the instrument response function for the experiments on the $6a_0^2$ band of pyridine to be 3.8 ps. Beside some day-to-day fluctuations it depended mostly on the wavelength and lay in general between 3 and 4 ps. In our experiments on the allyl radical we employed the second harmonic, shifted in frequency by stimulated Raman scattering (SRS). As the SRS process shortens the pulse by a factor of 2, the cross correlation is expected to be slightly smaller. It is also dominated by the Ti:Sa third harmonic, limiting the time-resolution of the system again to 3–4 ps.

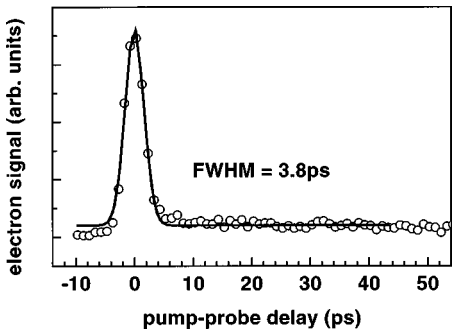

FIG. 13. In the photoelectron spectrum of pyridin a peak at 550 ns due to fast electrons originating from a $[3+1']$ process can be identified. Analyzing that peak as a function of the pump–probe delay yields the zero in time as well as the instrument response function.

IV. CONCLUSION

In this paper we presented experimental results on the nonradiative decay of the UV bands of the allyl radical, C_3H_5, as measured in a molecular beam of cold radicals. Lifetimes for all vibrational states between 250 and 238 nm, the whole range previously assigned by nanosecond-MPI spectroscopy, were determined by picosecond time-resolved photoelectron spectroscopy in a magnetic bottle using $[1+1']$ and $[2+1']$ excitation schemes. It was shown that this method is well suited for an investigation of the photophysics of organic radicals. The experimental setup as well as the advantages of the technique, background-free detection of time-dependent signals and the possibility to deduce the order of the processes from the spectra, were discussed. We observed lifetimes ranging from around 20 ps for the *B* 0_0^0 state at 249.7 nm, down to 9 ps for the *D* 7_0^1 band at 238 nm, in agreement with the increasing density of states. For the *C* 0_0^0 state a lifetime of 15 ps was found, 25% shorter than the lifetimes of the neighboring states. We interpreted the decay of the UV bands as being due to internal conversion, either directly to the ground state, or via the *A*-state, leading to the formation of hot ground state radicals. From the sharp photoelectron spectra we deduced information on the allyl cation, which has a geometry very similar to the *C*-state. The best fit to the spectrum from the *C*-state origin was obtained assuming a slight decrease in the CC bond length from 1.385 Å to 1.37 Å and a CCC bond angle of 116°, employing the *ab initio* frequencies of 1350, 1080, and 450 cm^{-1} for the ionic modes v_5^+, v_6^+, and v_7^+.

For a calibration of our experimental setup measurements on the S_1 state of pyridine were carried out, that allowed us to extract an instrument response function. The rate for internal conversion in pyridine is in good agreement with earlier experiments.

ACKNOWLEDGMENTS

We are indebted to Professor P. Chen for the generous support of this work and numerous helpful discussions. Financial support by the Schweizerische Nationalfonds and the ETH Zürich is gratefully acknowledged. We would like to thank H.-J. Deyerl for his help with the *ab initio* calculations on the allyl cation and D. Lührs for assistance in some of the measurements.

[1] S. D. Thomas, A. Bhargava, P. R. Westmoreland, R. P. Lindstedt, and G. Skevis, Bull. Soc. Chim. Belg. **105**, 501 (1996).
[2] K. M. Leung and R. P. Lindstedt, Combust. Flame **102**, 129 (1995).
[3] E. Hirota, C. Yamada, and M. Okunishi, J. Chem. Phys. **97**, 2963 (1992).
[4] J. D. Getty, M. J. Burmeister, S. G. Westre, and P. B. Kelly, J. Am. Chem. Soc. **113**, 801 (1991).
[5] G. Maier, H. P. Reisenauer, B. Rohde, and K. Dehnicke, Chem. Ber. **116**, 732 (1983).
[6] C. L. Currie and D. A. Ramsey, J. Chem. Phys. **45**, 488 (1966).
[7] A. B. Callear and H. K. Lee, Trans. Faraday Soc. **64**, 308 (1968).
[8] J. W. Hudgens and C. S. Dulcey, J. Phys. Chem. **89**, 1505 (1985).

[9] A. D. Sappey and J. C. Weisshaar, J. Phys. Chem. **91**, 3731 (1987).
[10] D. W. Minsek, J. A. Blush, and P. Chen, J. Phys. Chem. **96**, 2025 (1992).
[11] J. A. Blush, D. W. Munsek, and P. Chen, J. Phys. Chem. **96**, 10150 (1992).
[12] D. W. Minsek and P. Chen, J. Phys. Chem. **97**, 13375 (1993).
[13] J. D. Getty, X. Liu, and P. B. Kelly, J. Phys. Chem. **96**, 10155 (1992).
[14] J. D. Getty, X. Liu, and P. B. Kelly, Chem. Phys. Lett. **201**, 236 (1993).
[15] T.-K. Ha, H. Baumann, and J. F. M. Oth, J. Chem. Phys. **85**, 1438 (1986).
[16] N. Nakashima and K. Yoshihara, Laser Chem. **7**, 177 (1987).
[17] K. Holtzhauer, C. Cometta-Morini, and J. F. M. Oth, J. Phys. Org. Chem. **3**, 219 (1990).
[18] GAUSSIAN 94, Revision C.3, M. J. Frisch, G. W. Trucks, H. B. Schlegel, P. M. W. Gill, B. G. Johnson, M. A. Robb, J. R. Cheeseman, T. Keith, G. A. Petersson, J. A. Montgomery, K. Raghavachari, M. A. Al-Laham, V. G. Zakrzewski, J. V. Ortiz, J. B. Foresman, J. Cioslowski, B. B. Stefanov, A. Nanayakkara, M. Challacombe, C. Y. Peng, P. Y. Ayala, W. Shen, M. W. Wong, J. L. Andres, E. S. Replogle, R. Gomperts, R. L. Martin, D. J. Fox, J. S. Binkley, D. J. Defrees, J. Baker, J. P. Stewart, M. Head-Gordon, C. Gonzalez, and J. A. Pople, Gaussian, Inc., Pittsburgh, PA, 1995.
[19] P. Merlet, S. D. Peyerimhoff, R. J. Buenker, and S. Shih, J. Am. Chem. Soc. **96**, 959 (1974).
[20] T. Schultz and I. Fischer, J. Chem. Phys. **107**, 8197 (1997).
[21] H.-J Deyerl, T. Gilbert, I. Fischer, and P. Chen, J. Chem. Phys. **107**, 3329 (1997).
[22] A. H. Zewail, *Femtochemistry* (World Scientific, Singapore, 1994), Vols. 1 and 2.
[23] A. H. Zewail, J. Phys. Chem. **100**, 12701 (1996).
[24] *Femtosecond Chemistry*, edited by J. Manz and L. Wöste (VCH, Weinheim, 1995).
[25] T. Baumert, M. Grosser, R. Thalweiser, and G. Gerber, Phys. Rev. Lett. **67**, 3753 (1991).
[26] T. Baumert, C. Röttgermann, C. Rothenfusser, R. Thalweiser, V. Weiss, and G. Gerber, Phys. Rev. Lett. **69**, 1512 (1992).
[27] S. Wolf, G. Sommerer, S. Rutz, E. Schreiber, T. Leisner, L. Wöste, and R. S. Berry, Phys. Rev. Lett. **74**, 4177 (1995).
[28] J. B. Pallix and S. D. Colson, Chem. Phys. Lett. **119**, 38 (1985).
[29] J. M. Smith, C. Lakshminarayan, and J. L. Knee, J. Chem. Phys. **93**, 4475 (1990).
[30] J. A. Syage, Chem. Phys. Lett. **202**, 227 (1993).
[31] I. Fischer, M. J. J. Vrakking, D. M. Villeneuve, and A. Stolow, Chem. Phys. **207**, 331 (1996).
[32] A. Assion, M. Geisler, J. Helbing, V. Seyfried, and T. Baumert, Phys. Rev. A **54**, R4605 (1996).
[33] M. Seel and W. Domcke, J. Chem. Phys. **95**, 7806 (1991).
[34] M. Braun, C. Meier, and V. Engel, J. Chem. Phys. **105**, 530 (1996).
[35] D. R. Cyr and C. C. Hayden, J. Chem. Phys. **104**, 771 (1996).
[36] V. Blanchet and A. Stolow, J. Chem. Phys. **108**, 4371 (1998).
[37] K. Müller-Dethlefs and E. W. Schlag, Annu. Rev. Phys. Chem. **42**, 109 (1991).
[38] T. Baumert, R. Thalweiser, and G. Gerber, Chem. Phys. Lett. **209**, 29 (1993).
[39] I. Fischer, D. M. Villeneuve, M. J. J. Vrakking, and A. Stolow, J. Chem. Phys. **102**, 5566 (1995).
[40] M. R. Dobber, W. J. Buma, and C. A. deLange, J. Phys. Chem. **99**, 1671 (1995).
[41] M. R. Dobber, W. J. Buma, and C. A. deLange, J. Chem. Phys. **99**, 836 (1993).
[42] B. J. Greenblatt, M. T. Zanni, and D. M. Neumark, Science **276**, 1675 (1997).
[43] I. Fischer and T. Schultz, Appl. Phys. B: Lasers Opt. **B64**, 15 (1997).
[44] P. Kruit and F. H. Read, J. Phys. E **16**, 313 (1983).
[45] D. W. Minsek and P. Chen, J. Phys. Chem. **94**, 8399 (1990).
[46] C. A. deLange, in *High Resolution Photoionization and Photoelectron Studies*, edited by I. Powis, T. Baer, and C.-Y. Ng (Wiley, New York, 1995).
[47] P. Chen, S. D. Colson, W. A. Chupka, and J. A. Berson, J. Phys. Chem. **90**, 2319 (1986).
[48] D. W. Kohn, H. Clauberg, and P. Chen, Rev. Sci. Instrum. **63**, 4003 (1992).
[49] H.-J. Deyerl, I. Fischer, and P. Chen (in preparation).
[50] M. Klessinger and J. Michl, *Excited States and Photochemistry of Organic Molecules* (VCH, Weinheim, 1995).
[51] M. Bixon and J. Jortner, J. Chem. Phys. **48**, 715 (1968).
[52] F. A. Houle and J. L. Beauchamp, J. Am. Chem. Soc. **100**, 3290 (1978).
[53] K. Kimura, Adv. Chem. Phys. **60**, 161 (1985).
[54] P. Chen, in *Unimolecular and Bimolecular Reaction Dynamics*, edited by C. Y. Ng, T. Baer, and I. Powis (Wiley, New York, 1994).
[55] GAUSSIAN 94 (Revision A.1), M. J. Frisch *et al.*, Gaussian Inc., Pittsburgh, Pennsylvania 1995.
[56] I. Yamazaki, T. Murao, T. Yamanaka, and K. Yoshihara, Faraday Discuss. Chem. Soc. **75**, 395 (1983).